

Asymptotics of three-body bound state radial wave functions of halo nuclei involving two charged particles

R. Yarmukhamedov

E-mail: rakhim@inp.uz

Institute of Nuclear Physics, Tashkent 100214, Uzbekistan

Abstract

Asymptotic expressions for the radial and full wave functions of a three-body bound halo nuclear system with two charged particles in relative coordinates are obtained in explicit form, when the relative distance between two particles tends to infinity. The obtained asymptotic forms are applied to the analysis of the asymptotic behavior of the three-body ($pn\alpha$) wave functions for the halo ($E^*=3.562$ MeV, $J^\pi=0^+$, $T=1$) state of ${}^6\text{Li}$ derived by D. Baye within the Lagrange-mesh method for two forms of the αN -potential. The agreement between the calculated wave function and the asymptotic formula is excellent for distances up to 30 fm. Information about the values of the three-body asymptotic normalization functions is extracted. It is shown that the extracted values of the three-body asymptotic normalization function are sensitive to the form of the αN -potential. The mirror symmetry is revealed for the three-body asymptotic normalization functions derived for the isobaric (${}^6\text{He}, {}^6\text{Li}^*$) pair.

1 INTRODUCTION

Study of structure of light exotic nuclei, lying near the drip lines and so-called halo nuclei is one of the most interesting topics of low-energy nuclear physics [1–13]. It has revealed a number of features inherent only for these nuclei but not for normal (non-halo) nuclei, such as rather low separation energies of the external (“valence”) nucleons, large radii and narrow peaks observed in the breakup probability distribution. Two-nucleon halo nuclei are particularly striking since the lowest breakup channel is a three-body (core+“valence” nucleons) channel because of the fact that their two-body subsystems are unbound. Therefore, for these nuclei a main term of the asymptotics of wave functions must be determined by proper three-body asymptotics [14].

For more than ten years several works have been devoted to the study of the asymptotics of three-body bound state radial wave functions of halo nuclei [15–19]. In Refs.[15, 16], the asymptotic expressions have been derived for three-body systems with two neutrons for the case of short-range (nuclear) interactions. These asymptotics were derived in the context of hyperspherical coordinates for large values of the hyperradius R ($R \rightarrow \infty$), which means that either both of the Jacobi coordinates tend to infinity [17] or one of them tends to infinity and another of them is very small [16]. In [17], the result of [15] was generalized for three-body systems including two charged particles with taking into account Coulomb-nuclear interactions. The obtained asymptotic expressions contain an exponential function depending on the hyperradius R [14] but also involve a factor that can influence noticeably the asymptotic values of the three-body wave function for some directions in the configuration space determined by the hyperangle φ , where $\varphi = \arctan(y/x)$ (x and y are a pair of modified Jacobi

coordinates [14]). In Refs.[15, 16] and [17], these asymptotic expressions have been compared with the asymptotic behaviour of three-body ($nn\alpha$ and $\alpha\alpha n$) radial wave functions of the ${}^6\text{He}$ and ${}^9\text{Be}$ nuclei respectively derived in Refs.[20] and [21] within the framework of the multicluster stochastic dynamical model, respectively, where only two forms for the $n\alpha$ and $\alpha\alpha$ potentials are used. In Refs. [15–17], information was obtained about the three-body asymptotic normalization function (TBANF) as a function of the hyperangle φ . However, as is revealed in [15–17], the three-body radial wave functions of the ${}^6\text{He}$ and ${}^9\text{Be}$ nuclei [20, 21] have a correct asymptotic behaviour in an asymptotical region within the interval with narrow width. Besides, the binding energies of ${}^6\text{He}$ and ${}^9\text{Be}$ nuclei in the $(\alpha + 2n)$ -and $(2\alpha + n)$ -channels calculated in [20] and [21], respectively, differ noticeably from the experimental ones and, consequently, this circumstance may also noticeably influence the TBANFs [15–17].

In Ref.[18], the asymptotic expression has been derived for three-body radial wave functions of the halo nucleus with two valence neutrons in the context of the relative core-neutron coordinates for large values of each of them. It was revealed that the asymptotic expression obtained in [18] is not directly comparable to that derived in [15, 16] but it becomes equivalent to the asymptotic form derived in [15, 16] when the core is heavy. As a result, in Ref.[18], information about the values of the TBANFs has been obtained by means of comparative analysis of the obtained asymptotic forms with the asymptotic behavior of the corresponding model three-body ($nn\alpha$) wave functions for the ${}^6\text{He}$ nucleus derived within the Lagrange-mesh technique [3, 22] by using the αn potential taken from [23]. There it was shown that the Lagrange-mesh approximate wave function for the bound ${}^6\text{He}$ state is in good agreement with the asymptotic expression over larger values of the relative core-neutron coordinates (up to 20 fm) and information was obtained about the TBANF as a function of the ratio of the relative core-neutron coordinates. It should be noted that in [3, 22] the binding energy calculated for the ground state of ${}^6\text{He}$ is in excellent agreement with the experimental one for the employed nn and $n\alpha$ potentials.

In this connection it should be emphasized that the TBANF is a fundamental characteristic of the three-body bound system, which plays the same role as the asymptotic normalization coefficient of the radial wave function for the two-body bound system [24, 25]. Consequently, the TBANF is determined by the dynamics of strong interactions and, so, carries information about two-particle (nuclear) interactions in the three-body bound system. For example, as is shown in [15, 16] and [17], the extracted values of the TBANFs for the ${}^6\text{He}$ and ${}^9\text{Be}$ nuclei are highly sensitive to the forms of the αn and $\alpha\alpha$ potentials, respectively. Consequently, knowledge of the TBANF, which plays an important role in nuclear structure, allows one to get the information both on the three-body structure of halo nuclei and on types of two-particle (cluster-cluster, cluster-nucleon and nucleon-nucleon) interactions. Besides, as is shown in [26], the anomalous asymptotics of radial overlap integrals for bound systems a of four bodies in the $(b+c)$ -channel is expressed in terms of the TBANF. Therefore, systematic collection of data about TBANFs for different halo nuclei must be extremely encouraged now.

In the present work, the asymptotic behavior of the radial wave functions of a three-body bound (123)-system involving two charged particles is studied for the large relative coordinates r_{13} and r_{23} . The results are compared with the Lagrange-mesh approximate three-body ($pn\alpha$) radial wave functions derived by D. Baye [27] for the halo ($E^*=3.562$ MeV; $J^\pi = 0^+$; $T = 1$) state of ${}^6\text{Li}$, which is the isobar-analog one for the ground state of ${}^6\text{He}$ for which $J^\pi = 0^+$ and $T = 1$ also.

The content of this paper is as follows. In Section 2, the asymptotic expression for the radial component of three-body wave function is derived. In Section 3, the asymptotic formula is used for testing the asymptotic behavior of the partial waves of the three-body ($pn\alpha$) wave function for the halo ($E^*=3.562$ MeV) state of the ${}^6\text{Li}$ nucleus by using two kinds of the αN potential, which is

briefly described in Appendix B. In Section 3, the information about the TBANFs is also analysed and discussed. Conclusion are given in Section 4 and the asymptotic formula for the total three-body wave function is derived in Appendix A.

2 Asymptotic behavior of three-body radial wave functions with two charged particles

One considers the bound three-body system (123) consisting of two “valence” nucleons and two charged particles (say, particle 1 and a core 3). Let us write $\mathbf{r}_{ij} = \mathbf{r}_i - \mathbf{r}_j$ for the relative radius vector and \mathbf{q}_{ij} for corresponding relative momentum, where \mathbf{r}_k is a radius vector of the center of mass of the particle k . If m_j is the mass of particle j , we denote $\mu_{ij} = m_i m_j / m_{ij}$ and $\mu_{(ij)k} = m_{ij} m_k / m$ the reduced masses of the ij and $(ij)k$ systems, respectively, where $m_{ij} = m_i + m_j$ and $m = m_1 + m_2 + m_3$. The ${}^6\text{Li}(pn\alpha)$ nucleus considered within a three-body model can be used as an example.

The Fourier transformation for the radial three-body wave functions $\Psi_\nu(r_{23}, r_{13})$ can be presented to the form

$$\Psi_\nu(r_{23}, r_{13}) = \frac{(-1)^{l_{23}+l_{13}+1}}{(2\pi)^4} \frac{1}{r_{23}r_{13}} \times \int_{-\infty}^{\infty} dq_{23} q_{23} e^{iq_{23}r_{23}} f_{l_{23}}(q_{23}r_{23}) \int_{-\infty}^{\infty} dq_{13} q_{13} e^{iq_{13}r_{13}} f_{l_{13}}(q_{13}r_{13}) \Psi_\nu(q_{23}, q_{13}), \quad (1)$$

which is derived from Eqs. (6) and (15) of Ref. [18]. Herein $\Psi_\nu(q_{23}, q_{13})$ is the partial three-body wave functions in momentum space, which can be determined from the relation

$$\Psi_\nu(q_{23}, q_{13}) = (4\pi)^{-1} \int d\Omega_{\mathbf{q}_{23}} d\Omega_{\mathbf{q}_{13}} Y_{l_{23}l_{13}LM_L}^*(\hat{\mathbf{q}}_{23}, \hat{\mathbf{q}}_{13}) \Psi(\mathbf{q}_{23}, \mathbf{q}_{13}), \quad (2)$$

and

$$f_l(x) = \sum_{n=0}^l \frac{(l+n)!}{n!(l-n)!} \frac{1}{(-2ix)^n}, \quad (3)$$

where $\Psi(\mathbf{q}_{23}, \mathbf{q}_{13})$ is the total three-body wave function in the momentum representation, $\nu = \{l_{23}l_{13}Ls_{12}S\}$, l_{ij} is the relative orbital momentum of particles i and j ; $\mathbf{L} = \mathbf{l}_{23} + \mathbf{l}_{13}$, $\mathbf{s}_{12} = \mathbf{s}_1 + \mathbf{s}_2$ and $\mathbf{S} = \mathbf{s}_{12} + \mathbf{s}_3$; \mathbf{s}_j is the spin of particle j and $Y_{l_{23}l_{13}LM_L}^*(\hat{\mathbf{q}}_{23}, \hat{\mathbf{q}}_{13})$ is the eigenstates of the square of the total orbital angular momentum \mathbf{L} of the three-body (123) system and of its projection L_z along the z axis, which has the form

$$Y_{l_{23}l_{13}LM_L}(\hat{\mathbf{q}}_{23}, \hat{\mathbf{q}}_{13}) = \sum_{\nu_{23}\nu_{13}} C_{l_{23}\nu_{23}l_{13}\nu_{13}}^{LM_L} Y_{l_{23}\nu_{23}}(\hat{\mathbf{q}}_{23}) Y_{l_{13}\nu_{13}}(\hat{\mathbf{q}}_{13}) \quad (4)$$

in which $C_{a\alpha b\beta}^{\gamma}$ is a Clebsh-Gordan coefficient and $\hat{\mathbf{q}}_{ij} = \mathbf{q}_{ij}/q_{ij}$.

The momentum-space wave function $\Psi(\mathbf{q}_{23}, \mathbf{q}_{13})$ is related to the vertex function $W(\mathbf{q}_{23}, \mathbf{q}_{13})$ for the virtual decay

$$(123) \rightarrow 1 + 2 + 3 \quad (5)$$

by the relation [28]

$$\Psi(\mathbf{q}_{23}, \mathbf{q}_{13}) = -\frac{W(\mathbf{q}_{23}, \mathbf{q}_{13})}{\varepsilon + \varepsilon_a}. \quad (6)$$

Herein the energy ε reads [3]

$$\varepsilon = \frac{\mathbf{q}_{13}^2}{2\mu_{(23)1}} + \frac{(\mathbf{q}_{23} + \lambda_2 \mathbf{q}_{13})^2}{2\mu_{23}} \quad (7)$$

$$= \frac{\mathbf{q}_{23}^2}{2\mu_{(31)2}} + \frac{(\mathbf{q}_{13} + \lambda_1 \mathbf{q}_{23})^2}{2\mu_{31}}, \quad (8)$$

where $\lambda_1 = m_1/m_{31}$ and $\lambda_2 = m_2/m_{23}$, and ε_a is the binding energy of the system $a \equiv (123)$ in respect to the virtual decay (5) ($\varepsilon_a > 0$). We use $\hbar = c = 1$ throughout.

According to Ref.[14], if, in the bound (123)-system, two-particle subsystem (ij) ($ij=12,23,31$) can be bound with the binding energy ε_{ij} with respect to the $(i+j)$ -channel, the vertex function $W(\mathbf{q}_{23}, \mathbf{q}_{13})$ has so-called two-particle singularities as a function of the relative kinetic energy of the particles i and j , E_{ij} , at $E_{ij} = -\varepsilon_{ij}$. For the two-particle (12)-and (23)-subsystems, where the Coulomb interactions are absent, these two-particle singularities are pole ones, and for the two-particle (13)-subsystem the two-particle singularity is a power branch point arising due to the Coulomb interaction [29]. Besides, according to Refs.[14, 30], the vertex function $W(\mathbf{q}_{23}, \mathbf{q}_{13})$ has the three-body branch point singularity at $\varepsilon = -\varepsilon_a$. As seen from Eq.(6), the wave function $\Psi(\mathbf{q}_{23}, \mathbf{q}_{13})$ possesses the same singularities as the vertex function $W(\mathbf{q}_{23}, \mathbf{q}_{13})$.

In the general case the asymptotic form of the radial wave function $\Psi_\nu(r_{23}, r_{13})$ at $r_{23} \rightarrow \infty$ (or $r_{13} \rightarrow \infty$) is determined by both the two-body cluster singularities, which are associated with a formation of possible bound states in the two-particle subsystems [14], and by the three-body singularity at $\varepsilon = -\varepsilon_a$ of the partial wave functions in the momentum space $\Psi_\nu(q_{23}, q_{13})$. Explicit form of the cluster asymptotic can easily be derived by using the results of Ref.[14]. But, as a rule, two-body (ij) subsystem in bound three-body (123) halo nuclei are unbound, for example, the ${}^6\text{Li}(pn\alpha)$ nucleus in the second excited ($E^*=3.562$ MeV) state being the isobar-analog to the ground state of ${}^6\text{He}(nn\alpha)$. For such nuclei an asymptotic form of the three-body wave function is determined by the proper three-body asymptotics of function $\Psi_\nu(r_{23}, r_{13})$ at $r_{23} \rightarrow \infty$ (or $r_{13} \rightarrow \infty$). Therefore, here we are interested in the asymptotic expression for $\Psi_\nu(r_{23}, r_{13})$ at $r_{23} \rightarrow \infty$ (or $r_{13} \rightarrow \infty$) determined by means of the extraction of a contribution from the aforesaid three-body branch point singularity into the radial wave function $\Psi_\nu(r_{23}, r_{13})$ given by Eqs.(1), (2) and (6). To this end, one can make use in Eq. (6) the following singular part at $\varepsilon \rightarrow -\varepsilon_a$, $W^{(s)}(\mathbf{q}_{23}, \mathbf{q}_{13})$, of the vertex function $W(\mathbf{q}_{23}, \mathbf{q}_{13})$ [17, 30]:

$$W(\mathbf{q}_{23}, \mathbf{q}_{13}) \simeq W^{(s)}(\mathbf{q}_{23}, \mathbf{q}_{13}) = \Gamma(1 - \eta_a(q_{13})) \tilde{W}(\mathbf{q}_{23}, \mathbf{q}_{13}) \left(\frac{\varepsilon + \varepsilon_a}{4\varepsilon_a} \right)^{\eta_a(q_{13})}, \quad \varepsilon \rightarrow -\varepsilon_a, \quad (9)$$

where $\eta_a(q_{13}) = iz_1 z_3 e^2 \mu_{13}/q_{13}$, $z_j e$ is a charge of the particle j , and the function $\tilde{W}(\mathbf{q}_{23}, \mathbf{q}_{13})$ at the point $\varepsilon = -\varepsilon_a$ is regular part of the vertex function $W(\mathbf{q}_{23}, \mathbf{q}_{13})$, which coincides with the on-shell vertex function (OSVF) for the virtual decay (5) [30], i.e., with a value of the vertex function $W(\mathbf{q}_{23}, \mathbf{q}_{13})$ in which its arguments satisfy the relation $\mathbf{q}_{23}^2/2\mu_{(13)2} + (\mathbf{q}_{13} + \lambda_1 \mathbf{q}_{23})^2/2\mu_{13} = -\varepsilon_a$.

Taking into account the expressions (6) and (7), one can perform the integration over the angular variables $\Omega_{\mathbf{q}_{23}}$ and $\Omega_{\mathbf{q}_{13}}$ in Eq.(2). To this end, in Eq.(9), one makes use of the partial wave expansion for the OSVF:

$$\tilde{W}(\mathbf{q}_{23}, \mathbf{q}_{13}) = 4\pi \sum_{l'_{23} l'_{13} L' M_{L'}} Y_{l'_{23} l'_{13} L' M_{L'}}(\hat{\mathbf{q}}_{23}, \hat{\mathbf{q}}_{13}) W_{l'_{23} l'_{13} L' s_{12} S}(q_{23}, q_{13}), \quad (10)$$

where $W_{l'_{23}l'_{13}L's_{12}S}(q_{23}, q_{13})$ is a partial OSVF, and of the following presentation for the function $[(\varepsilon + \varepsilon_a)/4\varepsilon_a]^{\eta_a(q_{13})}/(\varepsilon + \varepsilon_a)$:

$$\frac{1}{\varepsilon_a + \varepsilon} \left(\frac{\varepsilon + \varepsilon_a}{4\varepsilon_a} \right)^{\eta_a(q_{13})} = 4\pi \sum_{L''M_{L''}} A_{L'';\eta_a(q_{13})}(q_{23}, q_{13}) Y_{L''M_{L''}}^*(\hat{\mathbf{q}}_{23}) Y_{L''M_{L''}}(\hat{\mathbf{q}}_{13}). \quad (11)$$

Herein the function $A_{L'';\eta_a(q_{13})}(q_{23}, q_{13})$ is determined by the relation

$$A_{L'';\eta_a(q_{13})}(q_{23}, q_{13}) = \frac{1}{2} \int_{-1}^1 P_{L''}(z) \left(\frac{\varepsilon + \varepsilon_a}{4\varepsilon_a} \right)^{\eta_a(q_{13})} \frac{dz}{\varepsilon_a + \varepsilon} \quad (12)$$

$$= \frac{(-1)^{L''}}{4\varepsilon_a} \left(\frac{4m_3\varepsilon_a}{q_{23}q_{13}} \right)^{1-\eta_a(q_{13})} \frac{e^{i\pi\eta_a(q_{13})}}{\Gamma(1-\eta_a(q_{13}))} [\zeta^2(q_{23}, q_{13}) - 1]^{\eta_a(q_{13})/2} Q_{L''}^{-\eta_a(q_{13})}[\zeta(q_{23}, q_{13})], \quad (13)$$

where

$$\varepsilon + \varepsilon_a = \frac{q_{23}q_{13}}{m_3} [\zeta(q_{23}, q_{13}) + z], \quad (14)$$

$$\zeta(q_{23}, q_{13}) = \frac{q_{13}^2 + \lambda_1 \lambda_2^{-1} (q_{23}^2 + \sigma \kappa^2)}{2\lambda_1 q_{23} q_{13}} \quad (15)$$

in which $\kappa = \sqrt{2\mu_{(23)1}\varepsilon_a}$, $\sigma = \mu_{23}/\mu_{(23)1} = (1 - \lambda_1 \lambda_2) \lambda_2 / \lambda_1$ and $Q_{L''}^\eta(x)$ is the associate Legendre function of the second kind [31]. Note that $\zeta(q_{23}, q_{13}) > 1$. The integration in Eq.(12) has been performed by using the formula (A.3) of Ref.[29]. Now the integration over the angle variables $\Omega_{\mathbf{q}_{23}}$ and $\Omega_{\mathbf{q}_{13}}$ can be performed by inserting the expressions (10) and (11) in the r.h.s. of Eq.(2). After that, the expression (1) for the three-body radial wave function with taking into account (13) can be reduced to the form

$$\begin{aligned} \Psi_\nu(r_{23}, r_{13}) = & -\frac{m_3}{(2\pi)^4} \frac{\sqrt{\hat{l}_{13}\hat{l}_{23}}}{r_{23}r_{13}} (-1)^{l_{13}+l_{23}+L} \sum_{\hat{l}'_{23}\hat{l}'_{13}\hat{L}'} \hat{L}' \sqrt{\hat{l}'_{13}\hat{l}'_{23}} I_{l_{23}l_{13}L\hat{l}'_{23}\hat{l}'_{13}\hat{L}'}(r_{23}, r_{13}) \\ & \times \begin{pmatrix} l_{23} & l'_{23} & L' \\ 0 & 0 & 0 \end{pmatrix} \begin{pmatrix} l_{13} & l'_{13} & L' \\ 0 & 0 & 0 \end{pmatrix} \left\{ \begin{matrix} l_{13} & l'_{13} & L' \\ l'_{23} & l_{23} & L \end{matrix} \right\} \end{aligned} \quad (16)$$

where $\hat{j} = 2j + 1$ and

$$\begin{aligned} I_{l_{23}l_{13}L\hat{l}'_{23}\hat{l}'_{13}\hat{L}'}(r_{23}, r_{13}) = & \int_{-\infty}^{\infty} dq_{23} e^{iq_{23}r_{23}} f_{l_{23}}(q_{23}r_{23}) \int_{-\infty}^{\infty} dq_{13} e^{iq_{13}r_{13}} f_{l_{13}}(q_{13}r_{13}) \left(\frac{q_{23}q_{13}}{4m_3\varepsilon_a} \right)^{\eta_a(q_{13})} \\ & \times e^{i\pi\eta_a(q_{13})} (\zeta^2(q_{23}, q_{13}) - 1)^{\eta_a(q_{13})/2} Q_{L'}^{-\eta_a(q_{13})}[\zeta(q_{23}, q_{13})] W_{l'_{23}l'_{13}Ls_{12}S}(q_{23}, q_{13}). \end{aligned} \quad (17)$$

The sought proper three-body asymptotic form for the radial wave function $\Psi_\nu(r_{23}, r_{13})$ at $r_{23} \rightarrow \infty$ (or $r_{13} \rightarrow \infty$) is determined by the aforesaid three-body singularity at the point $\varepsilon = \varepsilon_a$. This singularity is associated with singularities of the function $Q_{L'}^{-\eta_a(q_{13})}(\zeta(q_{23}, q_{13}))$ entering the integrand of Eq.(17), and is the power branch point [32]¹. The latter singularity is defined from the equation

$$\zeta(q_{23}, q_{13}) = \pm 1. \quad (18)$$

¹ Note that character of this singularity is a logarithm branch point one, when values of the Coulomb parameter $\eta_a(q_{13})$ are integer numbers [33].

The solution of Eq.(18) results in the power branch point type of singularities on the variable q_{23} located at

$$q_{23}^{(1,2)} = \pm \lambda_2 q_{13} + i\sqrt{\sigma} \sqrt{q_{13}^2 + \kappa^2} \quad (19)$$

and

$$q_{23}^{(3,4)} = \pm \lambda_2 q_{13} - i\sqrt{\sigma} \sqrt{q_{13}^2 + \kappa^2} \quad (20)$$

in the q_{23} plane (see Fig.1a).

To extract a contribution from these three-body singularities to the radial wave function $\Psi_\nu(r_{23}, r_{13})$ given by Eqs.(16) and (17), first, a deformation of the contour of integration into the upper half of the q_{23} -plane is carried out as shown in Fig.1a. Then, in the integrand of the obtained integrals, the function $e^{i\pi\eta_a(q_{13})}(\zeta^2 - 1)^{\eta_a(q_{13})/2} Q_{L'}^{-\eta_a(q_{13})}(\zeta)$ is written as

$$\begin{aligned} e^{i\pi\eta_a(q_{13})}(\zeta^2 - 1)^{\eta_a(q_{13})/2} Q_{L'}^{-\eta_a(q_{13})}(\zeta) &= \frac{\Gamma(L' - \eta_a(q_{13})) \Gamma(1 - L' + \eta_a(q_{13}))}{2\Gamma(1 + \eta_a(q_{13}))} \\ &\times [(-1)^{L'}(\zeta - 1)^{\eta_a(q_{13})} {}_2F_1(-L', L' + 1; 1 + \eta_a(q_{13}); \frac{1 - \zeta}{2}) - \\ &-(\zeta + 1)^{\eta_a(q_{13})} {}_2F_1(-L', L' + 1; 1 + \eta_a(q_{13}); \frac{1 + \zeta}{2})], \end{aligned} \quad (21)$$

where ${}_2F_1(a, b; c; x)$ is the hypergeometric function [31] and $\zeta \equiv \zeta(q_{23}, q_{13})$. The relation (21) can be obtained from the formula 3.3.2(15) of Ref.[33]. As a result, one can separate the parts of the integrals running along the cuts $C^{(1)}$ and $C^{(2)}$ in the q_{23} plane starting from $q_{23}^{(1)}$ to ∞ and from $q_{23}^{(2)}$ to $-\infty$, respectively, which correspond to the sought asymptotics of the three-body radial wave function $\Psi_\nu(r_{23}, r_{13})$. For $r_{23} \rightarrow \infty$ one extracts the contributions from the singular points $q_{23} = q_{23}^{(1)}$ and $q_{23} = q_{23}^{(2)}$ in the integrals over the contours $C^{(1)}$ and $C^{(2)}$, respectively. After that, the expression (17) can be reduced to the form

$$I_{l_{23}l_{13}l'_{23}l'_{13}L'L}(r_{23}, r_{13}) \approx \sum_{j=1}^2 (-1)^{j+1} I_{l_{23}l_{13}l'_{23}l'_{13}L'L}^{(j)}(r_{23}, r_{13}), \quad r_{23} \rightarrow \infty \quad (22)$$

$$\begin{aligned} I_{l_{23}l_{13}l'_{23}l'_{13}L'L}^{(j)}(r_{23}, r_{13}) &= \frac{\pi}{r_{23}} \xi_{L'}^{(j)} \int_{-\infty}^{\infty} dq_{13} e^{S^{(j)}(q_{13}; r_{23}, r_{13})} f_{l_{13}}(q_{13} r_{13}) \\ &\times f_{l_{23}}(q_{23}^{(j)} r_{23}) \left(\frac{q_{13}^2 + \kappa^2}{16\mu_{23}\mu_{(23)1}\varepsilon_a^2 r_{23}^2} \right)^{\eta_a(q_{13})/2} W_{l'_{23}l'_{13}Ls_{12}S}(q_{23}^{(j)}, q_{13}), \end{aligned} \quad (23)$$

$$S^{(j)}(q_{13}; r_{23}, r_{13}) = e^{iq_{13}r_{13} + iq_{23}^{(j)}r_{23}}, \quad (24)$$

where $\xi_{L'}^{(1)} = 1$ and $\xi_{L'}^{(2)} = (-1)^{L'}$. At the limit $r_{23} \rightarrow \infty$, the integration over q_{13} can now be performed by using the saddle-point method [34]. Before applying this method, it should be noted that the function $S(q_{23}; r_{23}, r_{13})$ in the exponent of the integrand of the integral (23) contains two parameters (r_{23} and r_{13}) and the saddle-point method for such type of an integral has been developed in Ref.[34] (see for details Section 7.3 of Chapter 4 of Ref.[34]). According to Ref.[34], the saddle points in Eq.(23) determined from equation

$$\frac{dS^{(j)}(q_{13}; r_{23}, r_{13})}{dq_{13}} = 0 \quad (25)$$

are given by

$$q_{13}^{(j)} = i2\mu_{(23)1}\sqrt{\epsilon_a} \frac{|r_{13} - (-1)^j \lambda_2 r_{23}|}{R^{(j)}(r_{23}, r_{13})}, \quad (26)$$

where

$$\begin{aligned} R^{(j)}(r_{23}, r_{13}) &= \sqrt{2\mu_{23}r_{23}^2 + 2\mu_{(23)1}(r_{13} - (-1)^j \lambda_2 r_{23})^2} = \\ &= \sqrt{2\mu_{13}r_{13}^2 + 2\mu_{(13)2}(r_{23} - (-1)^j \lambda_1 r_{13})^2} \end{aligned} \quad (27)$$

is a modified hyperradius [18]. It is noted that the expressions $R^{(1)}$ and $R^{(2)}$ are respectively the maximum and minimum values of the hyperradius R [14] for fixed values of r_{23} and r_{13} , when the angle between the relative coordinates varies. As is seen from Eqs. (A11) and (A12) of Appendix A, they coincide with R when three particles are aligned: $R^{(1)} = R$ when particles 1 and 2 are on the opposite sides of a core 3 and $R^{(2)} = R$ when they are on the same side. Inserting expression (26) into (19), one obtains

$$q_{23}^{(j)} = i2\mu_{(13)2}\sqrt{\epsilon_a} \frac{|r_{23} - (-1)^j \lambda_1 r_{13}|}{R^{(j)}(r_{23}, r_{13})}. \quad (28)$$

As a result, from Eqs.(16), (17), (22) and (23) the proper three-body asymptotic form of the radial wave function $\Psi_\nu(r_{23}, r_{13})$ is derived for $r_{23} \rightarrow \infty$ as

$$\begin{aligned} \Psi_\nu(r_{23}, r_{13}) &\simeq \Psi_\nu^{(as)}(r_{23}, r_{13}) = \{C_\nu^{(1)}(r)f_{l_{23}}(q_{23}^{(1)}r_{23})f_{l_{13}}(q_{13}^{(1)}r_{13})[2\sqrt{\epsilon_a}R^{(1)}(r_{23}, r_{13})]^{-\eta_a(q_{13}^{(1)})} \\ &\quad \times \exp[-\sqrt{\epsilon_a}R^{(1)}(r_{23}, r_{13})]/[R^{(1)}(r_{23}, r_{13})]^{3/2} \\ &\quad - C_\nu^{(2)}(r)f_{l_{23}}(q_{23}^{(2)}r_{23})f_{l_{13}}(q_{13}^{(2)}r_{13})[2\sqrt{\epsilon_a}R^{(2)}(r_{23}, r_{13})]^{-\eta_a(q_{13}^{(2)})} \\ &\quad \times \exp[-\sqrt{\epsilon_a}R^{(2)}(r_{23}, r_{13})]/[R^{(2)}(r_{23}, r_{13})]^{3/2}\}/r_{23}r_{13}, \end{aligned} \quad (29)$$

where $\eta_a(q_{13}^{(j)}) = iz_1 z_3 e^2 \mu_{31}/q_{13}^{(j)}$. The expression is also valid for $r_{13} \rightarrow \infty$ since the expressions for $q_{23}^{(j)}$, $q_{13}^{(j)}$ and $R^{(j)}$ do not change. This means that the asymptotic formula is valid when $r_{23} \rightarrow \infty$ and $r_{13} \rightarrow \infty$. However, similar to what it has been done in Ref.[18], in the derivation of the saddle points $q_{23}^{(j)}$ and $q_{13}^{(j)}$, one also implicitly assumes that the ratio $r = r_{13}/r_{23}$ is larger than λ_2 and smaller than $1/\lambda_1$.

In Eq.(29), the asymptotic normalization functions $C_\nu^{(j)}(r)$ are related to the partial OSVF , $W_{l'_{23}l'_{13}Ls_{12}S}(q_{23}^{(j)}, q_{13}^{(j)})$, by

$$\begin{aligned} C_\nu^{(j)}(r) &= N(-1)^{l_{13}+l_{23}+L} \sum_{l'_{23}l'_{13}L'} \xi_{L'}^{(j)} \hat{L}' \sqrt{\hat{l}_{13}\hat{l}_{23}\hat{l}'_{23}\hat{l}'_{13}} \\ &\quad \times W_{l'_{23}l'_{13}Ls_{12}S}(q_{23}^{(j)}, q_{13}^{(j)}) \begin{pmatrix} l_{23} & l'_{23} & L' \\ 0 & 0 & 0 \end{pmatrix} \begin{pmatrix} l_{13} & l'_{13} & L' \\ 0 & 0 & 0 \end{pmatrix} \left\{ \begin{matrix} l_{13} & l'_{13} & L' \\ l'_{23} & l_{23} & L \end{matrix} \right\}, \end{aligned} \quad (30)$$

where $N = (2\pi)^{-5/2} m_3(m_1 m_2 m_3/m)^{1/2} \epsilon_a^{1/4}$. It should be noted that for $\eta_a^{(j)} = 0$ the expression (29) coincides with that of Eq.(28) obtained in Ref.[18] for three-body (123) bound system with pure short range nuclear two-particle interactions.

As is seen from Eqs. (29) and (30), the asymptotics form for the three-body radial wave functions has the radial dependence quite different from that for the total three-body wave function derived

in Appendix A and given by Eqs. (A17)–(A19). Besides, the present asymptotic expression (29) is not directly comparable to relation derived in Ref.[17] for the Jacobi variables since the partial wave expansions are quite different. But, when particle 3 is very heavy ($m_3 \rightarrow \infty$, i.e. $\lambda_1 \rightarrow 0$ and $\lambda_2 \rightarrow 0$), similar to what it is done in [18], it can easily be shown that the expression (29) becomes equivalent to the asymptotic formula (11) of Ref.[17]. When m_3 is not large, these two expressions behave quite differently. The similar situation occurs for the leading term of Eq.(29) valid for $|q_{23}^{(j)} r_{23}| \gg 1$ and $|q_{13}^{(j)} r_{13}| \gg 1$ and the asymptotics form of Eq.(A17) valid at $R \rightarrow \infty$ for the total three-body wave function. In this case, both expressions have also the same radial dependence as $(2\sqrt{\varepsilon_a}R)^{-\eta_a} e^{-\sqrt{\varepsilon_a}R}/R^{5/2}$, where η_a is given by Eqs. (A12), (A14) and (A19) of Appendix A at $\lambda_2=0$.

As is also seen from Eq.(29), the proper three-body asymptotics of the bound state radial wave function $\Psi_\nu(r_{23}, r_{13})$ for $r_{23} \rightarrow \infty$ and $r_{13} \rightarrow \infty$ contains unknown functions $C_\nu^{(j)}(r)$ related to the partial OSVF $W_{\hat{p}_{23}\hat{p}_{13}Ls_{12}S}(q_{23}^{(j)}, q_{13}^{(j)})$ by Eq.(30). Consequently, as it was mentioned above, due to the fact that the partial OSVF is determined by the dynamics of strong two-particles interaction [35], knowledge of the factor $C_\nu^{(j)}(r)$ allows one to get the valuable information both on the three-body structure of halo nuclei and on types of two-particle (cluster-cluster, cluster-nucleon and nucleon-nucleon) interactions.

3 Analysis of the three-body wave functions for the second excited state of the ${}^6\text{Li}^*$ nucleus

In this section, the results of the comparative analysis of the asymptotic expression (29) with the approximate radial three-body wave functions for the halo ($E^*=3.562$ MeV) state of ${}^6\text{Li}$, which were derived by D. Baye [27] within the framework of the $pn\alpha$ three-body approach based on the Lagrange-mesh technique [36–39] and given by Eq. (B2) in Appendix B, are presented. These radial three-body wave functions were obtained using the central part of the Minnesota NN potential and two kinds of the αN potential denoted by the M1 and M2 models below (see, Appendix B also). The leading asymptotic expression for the three-body ($pn\alpha$) radial wave functions for ${}^6\text{Li}(E^*=3.562$ MeV) is determined by the expression (29), since there are no two-particle bound subsystems for the ${}^6\text{Li}(E^*=3.562$ MeV) nucleus within the three-body ($pn\alpha$) model. Note that, as it is mentioned above, this second excited state of the ${}^6\text{Li}$ nucleus is the isobar-analog for the ground state of the ${}^6\text{He}$ halo nucleus. Therefore, similar to that done in [18] for the ground state of ${}^6\text{He}$, it is of interest to find out to what extent the approximate radial wave functions [27] have correct asymptotic behavior in the asymptotic region ($r_{23} \rightarrow \infty$ and $r_{13} \rightarrow \infty$).

3.1 Results and discussion

The TBANFs $C_{Ll}^{(j)}(r)$ ($j=1$ and 2) are determined based on the same procedure as used in Ref.[18] for the ${}^6\text{He}(nn\alpha)$ nucleus, where the index ν is substituted by Ll since the quantum numbers summarized by index ν are fully determined by the values L and l . We consider value of r belonging to the interval $1.0 \lesssim r \lesssim 3.0$. This limit is connected with the fact that other values of r correspond to too large r_{23} values (for $r < 1$) for which the approximate wave function (B2) becomes inaccurate. For too small r_{23} values (too large r values) the asymptotic expression (29) is not valid. Therefore, the limit mentioned above for r (or r_{23} and r_{13}) leads to the fact that the tail of the amplitude of the three-body radial wave functions $\Psi_{Ll}(r_{23}, r_{13})$ corresponds to values of $r_{23} \equiv r_{n\alpha} \gtrsim 5$ fm and

$r_{13} \equiv r_{p\alpha} \gtrsim 14$ fm because of the small value of the binding energy ε and presence of the Coulomb $p\alpha$ interaction.

After a number of tests, we have found that the convenient procedure is to fix two coefficients $C_{Ll}^{(j)}(r)$ by fitting them to two values of the partial wave function separated by a distance Δr_{23} for a fixed r . The optimal values of Δr_{23} equal to from 2.00 till 2.25 fm seem to be adequate. Similarly to Ref. [18], we have searched for a region where the obtained values of the TBANF's $C_{Ll}^{(j)}(r)$ are stable within about 10%, and have then tested the validity of the obtained fit inside that region.

As the examples of the search, some values of r are displayed in Table 1 both for the M1 model and for the M2 model. The obtained values are shown as a function of different choices for fitting points (r_{23}, r_{13}) and $(r_{23} + \Delta r_{23}, r_{13} + r\Delta r_{23})$ for the dominant partial waves $(L, l)=(0,0), (0,1)$ and $(0,2)$ for spin $S=0$, and $(L, l)=(1,1)$ and $(1,2)$ for spin $S=1$. As shown in Table 1, different choices of the fitting points can be found, which lead to similar values of the coefficients $C_{Ll}^{(j)}(r)$. The similar situation occurs for other values of the ratio $r = r_{13}/r_{23}$. Strikingly, the ratio $C_{Ll}^{(2)}/C_{Ll}^{(1)}$ is very stable. This indicates that only the overall normalization of the numerical wave function is sensitive to the fitting points. The width Δ ($\Delta = r_{23}^{(max)} - r_{23}^{(min)}$) of interval for the variable r_{23} , within which the approximate wave function (B2) has a correct asymptotic behavior to within about 10%, is presented in the sixth and tenth columns of Table 1 for the M1 and M2 models, respectively. Table 1 shows that the width of the interval becomes wider with decreasing r and more narrow with increasing ratio r both for the M1 model and the M2 model. For example, for $L=0, l=0$ and $r=1.1$, the expressions (29) and (B2) agree within about 10% for r_{23} from about 14 to 24 fm for the M1 model and from about 14 to 27 fm for the M2 model. One notes that the same behavior is practically observed for $r_{13} = 1.0r_{23}$. For $r_{13} = 2.5r_{23}$, the fit is excellent from about 6 to 11.5 fm for the M1 model and from about 6 to 12.5 fm for the M2 model. One can observe that the width of the interval Δ becomes more narrow with increasing r and moves to smaller values of r_{23} . For the $L=0$ and $l=1$ partial wave an accuracy of about 10% is obtained up to r_{23} equal to from about 16 to about 23 fm for the M1 model and from about 16 to 24 fm for the M2 model at $r_{13} = 1.1r_{23}$. The same accuracy is reached from about 6 to 11 fm for the M1 model and from about 6 to 12 fm for the M2 model at $r_{13} = 2.4r_{23}$. Here one observes that the width Δ decreases with increasing r both for the M1 model and for the M2 model, but it moves to smaller values of r_{23} . For the small $L=1$ and $l=2$ component the quality of the agreement is reached from about 17 to 24 for the M1 model and about from 17 to 29 for the M2 model at $r_{13} = 1.3r_{23}$. Similar situation is observed for other values of r . To confirm this and for the visual convenience, Fig. 2 shows the ratio of the approximate wave function (B2) to the asymptotic form (29) as a function of r_{23} for different values of r , including the values of r not presented in Table 1, only for the M2 model.

It is seen here that, the width Δ depends both on values of r and on the form of the αN potential used. One also observes in Table 1 that the region where the fit is performed moves to larger distances when l increases. This reflects the fact that the centrifugal barrier pushes the asymptotic region to larger distances with increasing l . One notes that the influence of the centrifugal barrier on the asymptotic form (29) arises only for $l > 0$ and is determined by the multiplicative factors $f_{l23}(q_{23}^{(j)} r_{23}) f_{l13}(q_{13}^{(j)} r_{23})$. These factors play an important role for the good agreement (within 10%) between the approximate wave function (B2) and the asymptotic form (29) in the asymptotic region, similar to that for the ${}^6\text{He}(nn\alpha)$ nucleus shown in Refs. [18].

We have applied the fitting technique described above to the determination of the TBANFs for the halo ($E^*=3.562$ MeV) state of the ${}^6\text{Li}$ nucleus as a function of r under the model conditions described above. The recommended values of $C_{Ll}^{(j)}(r)$ for $j=1$ and 2 are presented in Figs. 3 and 4 by the

solid and dashed curves for the M1 and M2 models, respectively. Figs. 3 and 4 correspond to $L=0$ and 1, respectively. The curves correspond to the averaged arithmetical means of $C_{Ll}^{(j)}(r)$, which are obtained from those for which the approximate wave function and the asymptotic form agree within about $\pm 10\%$ for the different fitting points (r_{23}, r_{13}) and $(r_{23} + \Delta r_{23}, r_{13} + r \Delta r_{23})$. In all cases, one has $|C_{Ll}^{(1)}| > |C_{Ll}^{(2)}|$ similar to that found in [18] for the ${}^6\text{He}(\text{g.s.})$ nucleus. One notes that the extracted values of the TBANFs $C_{Ll}^{(j)}(r)$ show a noticeable sensitivity to the form of the αN potential, although the binding energies calculated in the M1 and M2 models are fairly close to each other (see Appendix B).

3.2 Comparison of the TBANFs for the isobaric (${}^6\text{He}$, ${}^6\text{Li}^*$) pair

It is now of interest to compare the TBANF values derived by us above for the leading components ($(Ll)=(0,1)$ and $(1,1)$) and the M2 model with those obtained in Ref.[18] for the ground state of ${}^6\text{He}(\text{g.s.})$. Note that, in Ref. [18] the TBANF values were obtained only for the nuclear αN and NN potentials used in the M2 model. For this purpose, we form the ratio $R_{Ll}^{(j)} \equiv R_{Ll}^{(j)}(r) = C_{Ll}^{(j)}({}^6\text{Li}^*)/C_{Ll}^{(j)}({}^6\text{He})$ as a function of r , where $C_{Ll}^{(j)}({}^6\text{Li}^*)$ denotes $C_{Ll}^{(j)}(r)$ for ${}^6\text{Li}(E^*=3.562 \text{ MeV})$ and $C_{Ll}^{(j)}({}^6\text{He})$ denotes $C_{Ll}^{(j)}(r)$ for ${}^6\text{He}(\text{g.s.})$. The results for the ratio are presented in Fig. 5. The uncertainty for each curve is about $\pm 14\%$, which is the average square error for the ratio $R_{Ll}^{(j)}$, which involves the uncertainties of the $C_{Ll}^{(j)}({}^6\text{Li}^*)$ and $C_{Ll}^{(j)}({}^6\text{He}(\text{g.s.}))$. As is seen from figures, the interval of changing the variable r can be divided in three parts (denoted by Ω_f , $f=1, 2$ and 3). In Ω_1 , a value of r changes from 1.0 to about 1.1 for which the values of $R_{Ll}^{(j)}$ are noticeably larger than 1. These values of r correspond to rather large values for the (r_{23}, r_{13}) pair, which are the fitting points providing the stable values of the $C_{Ll}^{(j)}({}^6\text{Li}^*)$. For example, $R_{01}^{(1)}=2.08\pm 0.29$ and $R_{01}^{(2)}=1.98\pm 0.28$ as well as $R_{11}^{(1)}=1.73\pm 0.24$ and $R_{11}^{(2)}=1.62\pm 0.23$ at $(r_{23}, r_{13})=(19.0 \text{ fm}, 19.0 \text{ fm})$ for $r=1.0$. In Ω_2 , a value of r changes within the interval $1.3 \lesssim r \lesssim 1.7$ for which the values of $R_{Ll}^{(j)}$ are quite close to 1. In Ω_2 , values of r_{23} and r_{13} decrease for the fitting points providing the stable values of the TBANFs $C_{Ll}^{(j)}({}^6\text{Li}^*)$. For example, $R_{01}^{(1)}=1.11\pm 0.16$ and $R_{01}^{(2)}=0.99\pm 0.14$ as well as $R_{11}^{(1)}=1.18\pm 0.17$ and $R_{11}^{(2)}=1.00\pm 0.14$ at $(r_{23}, r_{13})=(13.50 \text{ fm}, 17.55 \text{ fm})$ for $r=1.3$. At last, in Ω_3 , the values of $R_{Ll}^{(j)}$ are noticeably less than 1 for $r \gtrsim 1.9$. For these values r and the fitting points for the (r_{23}, r_{13}) pair, the values of r_{23} decrease and values of r_{13} increase. For example, $R_{01}^{(1)}=0.81\pm 0.11$ and $R_{01}^{(2)}=0.69\pm 0.10$ as well as $R_{11}^{(1)}=0.75\pm 0.10$ and $R_{11}^{(2)}=0.63\pm 0.10$ at $(r_{23}, r_{13})=(9.00 \text{ fm}, 18.9 \text{ fm})$ for $r=2.1$.

As is seen from here, the mirror symmetry for the TBANFs derived for the isobar-analog states of the isobaric (${}^6\text{He}$, ${}^6\text{Li}^*$) pair breaks up significantly in Ω_1 and Ω_3 . Apparently, this is connected with the fact that an influence of the Coulomb $p\alpha$ interaction upon the derived TBANFs $C_{Ll}^{(j)}({}^6\text{Li}^*)$ becomes noticeable for the values of r_{13} changing in Ω_1 and Ω_3 . Nevertheless, in Ω_2 , the mirror symmetry for the TBANF values derived for $C_{Ll}^{(j)}({}^6\text{Li}^*)$ and $C_{Ll}^{(j)}({}^6\text{He})$ occurs within their uncertainties. One of the main reason is the fact that the values of $r_{13}(=r_{p\alpha})$ for the fitting points in Ω_2 are less than those in Ω_1 and Ω_3 and, consequently, an influence of the Coulomb $p\alpha$ interaction decreases in Ω_2 with respect to that of the Coulomb $p\alpha$ interaction in Ω_1 and Ω_3 .

4 Conclusion

In this work, we have determined the asymptotic forms of the radial and total three- body (123) wave functions of halo nuclei with two charged particles (1 and a core 3) in core-nucleon coordinates. Although, such expressions are already known in hyperspherical (or Jacobi) coordinates [17, 30], we think that the present formulae are interesting because they allow a simpler physical visualization of the asymptotic behavior as a function of the two core-nucleon relative distances r_{23} and r_{13} . It is demonstrated that when the core is very heavy the derived asymptotic forms become equivalent to the corresponding asymptotic formulae [17, 30] for the Jacobi coordinates.

The asymptotic form obtained for the radial wave functions has been compared in different parts of asymptotic regions with the approximate wave functions derived by D. Baye [27] within the Lagrange-mesh approach for the halo ($E^*=3.562$ MeV) state of ${}^6\text{Li}(pn\alpha)$ using two kinds of the nuclear αN potential. The intervals of the r_{23} and r_{13} variables within which the approximate wave functions have a correct asymptotic behavior within about 10% have been determined.

One has used the region where the agreement between a radial wave function and the asymptotic expressions is excellent to deduce values for the TBANFs, $C_{Li}^{(1)}(r)$ and $C_{Li}^{(2)}(r)$, for the ${}^6\text{Li}^*(E^*=3.562$ MeV) nucleus depending on the ratio $r = r_{13}/r_{23}$. The shape of the asymptotic behavior is determined by the ratio $C_{Li}^{(2)}(r)/C_{Li}^{(1)}(r)$ and the overall normalization is sensitive to the fitting points. It is demonstrated that the values of the TBANFs are sensitive to the form of the αN potential used. Besides, it is revealed the region of changing the $(r_{n\alpha}, r_{p\alpha})$ pair where the mirror symmetry occurs for the TBANFs derived for the isobaric (${}^6\text{He}(\text{g.s.}), {}^6\text{Li}^*(E^*=3.562$ MeV)) pair.

The deduced three-body asymptotic functions are in principle observable quantities, for example, from an analysis of the experimental differential cross sections for the exchange $\alpha({}^6\text{Li}, \alpha){}^6\text{Li}(3.562$ MeV) and transfer $\alpha({}^3\text{He}, p){}^6\text{Li}(3.562$ MeV) reactions. Therefore, it would be interesting to compare present results with experimental ones. It would make it possible to choose the form of the αN potential by comparing the phenomenological values of $C_{Li}^{(j)}(r)$ ($j=1$ and 2) with these values obtained in the present work. They would allow one to get additional information about the form of the αN potential and to verify an accuracy of the approximate wave function (B2) as a source of reliable information on the $C_{Li}^{(j)}(r)$ asymptotic normalization functions. In this connection, it would be highly encouraged to do such an experiment.

ACKNOWLEDGEMENTS

The author is deeply grateful to D. Baye and L. D. Blokhintsev for reading a manuscript, discussions and general encouragement. The author thanks Y. Suzuki for interest and D. Baye for providing the numerical data calculated for the approximate three-body radial wave functions for ${}^6\text{Li}(E^*=3.562$ MeV). The work has been supported by The Academy of Sciences of the Republic of Uzbekistan under grant No. F2-FA-F177.

APPENDIX A: ASYMPTOTIC BEHAVIOR OF THE FULL THREE-BODY WAVE FUNCTION

Here, it is interesting to derive a proper three-body asymptotics of the total three-body wave function $\Psi(\mathbf{r}_{23}, \mathbf{r}_{13})$ at $r_{23} \rightarrow \infty$ (or $r_{13} \rightarrow \infty$) for the bound three-body ($a=(123)$) state directly using Fourier representation for the total three-body wave function. But, first one notes that in Refs.[14, 30] an asymptotic behavior of the total three-body wave function $\Psi(\mathbf{R})$ for $R \rightarrow \infty$ has been investigated by using the Fourier representation written through the six-dimensional vectors $\mathbf{R} = \{\mathbf{x}, \mathbf{y}\} [= \{R, \hat{\mathbf{R}}\}]$ and $\mathbf{P} = \{\mathbf{q}, \mathbf{p}\} [= \{P, \hat{\mathbf{P}}\}]$. Here $x = \sqrt{2\mu_{12}r_{12}}$ and $y = \sqrt{2\mu_{(12)3}r_{(12)3}}$ (\mathbf{q} and \mathbf{p}) are the modified coordinate Jacobi variables (conjugate momentums to them) [14]; $\hat{\mathbf{R}} = \{\hat{\mathbf{x}}, \hat{\mathbf{y}}, \varphi\}$; $R = \sqrt{x^2 + y^2}$ and $\varphi = \arctan(y/x)$ are the hyperradius and hyperangle in the configuration space, respectively; $\mathbf{r}_{(12)3}$ is the radius vector connecting the centers of masses of the (12)-pair and the particle 3; $P = \sqrt{q^2 + p^2}$ and $\hat{\mathbf{b}} = \mathbf{b}/b$ is a unit radius vector. In particular, it was shown in work of Ref.[30] that the derived asymptotic form $\Psi(\mathbf{R})$ at $R \rightarrow \infty$ contains a factor of OSVF for the virtual decay (11), which depends on the variables φ , $\hat{\mathbf{x}}$ (or $\hat{\mathbf{r}}_{12}$) and $\hat{\mathbf{y}}$ (or $\hat{\mathbf{r}}_{(12)3}$). Besides, in Ref.[30] the important relation between the total OSVF and the total three-body asymptotic normalization coefficient $C(\hat{\mathbf{R}})$ has also been found.

The Fourier transformation for the total wave function is written as

$$\Psi(\mathbf{r}_{23}, \mathbf{r}_{13}) = \int \frac{d\mathbf{q}_{23}}{(2\pi)^3} \frac{d\mathbf{q}_{13}}{(2\pi)^3} e^{i(\mathbf{r}_{23}\mathbf{q}_{23} + \mathbf{r}_{13}\mathbf{q}_{13})} \Psi(\mathbf{q}_{23}, \mathbf{q}_{13}) \quad (\text{A1})$$

$$= - \int \frac{d\mathbf{q}_{23}}{(2\pi)^3} e^{i(\mathbf{r}_{23} - \lambda_1 \mathbf{r}_{13})\mathbf{q}_{23}} I(\mathbf{q}_{23}; \mathbf{r}_{13}). \quad (\text{A2})$$

Herein the expressions (6), (8) and (9) as well as the substitution $\mathbf{q}'_{13} = \mathbf{q}_{13} + \lambda_1 \mathbf{q}_{23}$ in Eq.(A1) are used, where

$$\begin{aligned} I(\mathbf{q}_{23}; \mathbf{r}_{13}) &= \frac{1}{4\varepsilon_a} \int \frac{d\mathbf{q}'_{13}}{(2\pi)^3} e^{i\mathbf{r}_{13}\mathbf{q}'_{13}} \Gamma(1 - \eta_a(\mathbf{q}'_{13}, \mathbf{q}_{23})) \\ &\times W_a(-\mathbf{q}_{23}, -\mathbf{q}'_{13} + \lambda_1 \mathbf{q}_{23}) \left(\frac{q'^2_{13}/2\mu_{31} + q^2_{23}/2\mu_{(31)2} + \varepsilon_a}{4\varepsilon_a} \right)^{\eta_a(\mathbf{q}'_{13}, \mathbf{q}_{23})-1} \end{aligned} \quad (\text{A3})$$

and $\eta_a(q_{13}) \equiv \eta_a(\mathbf{q}'_{13}, \mathbf{q}_{23}) = iz_3 z_1 e^2 \mu_{31} / |\mathbf{q}'_{13} - \lambda_1 \mathbf{q}_{23}|$.

We consider the expression (A3) at $r_{13} \rightarrow \infty$ and perform integration over \mathbf{q}'_{13} in it. Similar to Refs.[14, 40], the leading term of the integrals over \mathbf{q}'_{13} at $r_{13} \rightarrow \infty$ is generated by the contribution from the three-body branch point singularity located at $\varepsilon = -\varepsilon_a$. Similar to what has been done in Ref.[40] (see for details, e.g., Section 6 of the Chapter 4 there) an estimation of the leading term of the integrals over \mathbf{q}'_{13} at $r_{13} \rightarrow \infty$ can be done by using the multidimensional method of stationary phase [34]. The stationary phase points are given by $\hat{\mathbf{q}}'_{13} = \pm \hat{\mathbf{r}}_{13}$. When the expression (A3) can be reduced to the form

$$\begin{aligned} I(\mathbf{q}_{23}; \mathbf{r}_{13}) &\simeq I^{(as)}(\mathbf{q}_{23}; \mathbf{r}_{13}) = \frac{1}{16i\pi^2 \varepsilon_a r_{13}} \int_{-\infty}^{\infty} d\mathbf{q}'_{13} q'_{13} e^{iq'_{13} r_{13}} \Gamma(1 - \eta_a(\hat{\mathbf{r}}_{13} \mathbf{q}'_{13}, \mathbf{q}_{23})) \\ &\times W_a(-\mathbf{q}_{23}, -\hat{\mathbf{r}}_{13} \mathbf{q}'_{13} + \lambda_1 \mathbf{q}_{23}) \left(\frac{q'^2_{13}/2\mu_{31} + q^2_{23}/2\mu_{(31)2} + \varepsilon_a}{4\varepsilon_a} \right)^{\eta_a(\hat{\mathbf{r}}_{13} \mathbf{q}'_{13}, \mathbf{q}_{23})-1} \end{aligned} \quad (\text{A4})$$

for $r_{13} \rightarrow \infty$, where $\eta_a(\hat{\mathbf{r}}_{13}q'_{13}, \mathbf{q}_{23}) = iz_3z_1e^2\mu_{31}/|\hat{\mathbf{r}}_{13}q'_{13} - \lambda_1\mathbf{q}_{23}|$. Then, one extracts contribution from the three-body branch point singularity located at $q'_{13} = iq'_{13}^{(o)}(q_{23}) \equiv i\sqrt{2\mu_{31}(q_{23}^2/2\mu_{(31)2} + \varepsilon_a)}$ of the integrand in (A4) by means of a deformation of the contour of integration into the upper half of the q'_{13} plane as plotted in Fig.1b. As a result, one can separate the part of integral running along the cut lying on the imaginary axis in the q'_{13} plane starting from $q'_{13}^{(o)}(q_{23})$ to ∞ that corresponds to the leading term of the expression (A4) at $r_{13} \rightarrow \infty$. After that, expression (A4) can be reduced to the form

$$I(\mathbf{q}_{23}; \mathbf{r}_{13}) \simeq I^{(as)}(\mathbf{q}_{23}; \mathbf{r}_{13}) \simeq \frac{1}{2\pi} \frac{\mu_{13}}{r_{13}} e^{ir_{13}q'^{(+)}(q_{23})} \times \left[\frac{q'^{(+)}(q_{23})}{4\mu_{31}\varepsilon_a r_{13}} \right]^{\eta_a(\hat{\mathbf{r}}_{13}q'^{(+)}(q_{23}), \mathbf{q}_{23})} W(-\mathbf{q}_{23}, -\hat{\mathbf{r}}_{13}q'^{(+)}(q_{23}) + \lambda_1\mathbf{q}_{23}), \quad r_{13} \rightarrow \infty. \quad (\text{A5})$$

By inserting the expression (A5) into the r.h.s. of Eq.(A2), the latter can be rewritten to the form

$$\Psi(\mathbf{r}_{23}, \mathbf{r}_{13}) \simeq \Psi^{(as)}(\mathbf{r}_{23}, \mathbf{r}_{13}) = \int d\mathbf{q}_{23} e^{r_{13}S(\mathbf{q}_{23}; \mathbf{r}_{23}, \mathbf{r}_{13})} h(\mathbf{q}_{23}; \mathbf{r}_{23}, \mathbf{r}_{13}) \quad (\text{A6})$$

for $r_{13} \rightarrow \infty$. Herein

$$h(\mathbf{q}_{23}; \mathbf{r}_{23}, \mathbf{r}_{13}) = -\frac{1}{(2\pi)^4} \frac{\mu_{31}}{r_{13}} \times \left(\frac{q_{23}^2/2\mu_{(31)2} + \varepsilon_a}{8\mu_{31}\varepsilon_a^2 r_{13}^2} \right)^{\eta_a(\hat{\mathbf{r}}_{13}q'^{(+)}(q_{23}), \mathbf{q}_{23})/2} W(-\mathbf{q}_{23}, -\hat{\mathbf{r}}_{13}q'^{(+)}(q_{23}) + \lambda_1\mathbf{q}_{23}), \quad (\text{A7})$$

$$S(\mathbf{q}_{23}; \mathbf{r}_{23}, \mathbf{r}_{13}) = i(\mathbf{r}_{23} - \lambda_1\mathbf{r}_{13})\mathbf{q}_{23}/r_{13} - q'^{(+)}(q_{23}). \quad (\text{A8})$$

At $r_{13} \rightarrow \infty$, the integration over \mathbf{q}_{23} can be performed by using the multidimensional saddle-point method [34]. The saddle points are determined from equations

$$\text{grad}_{\mathbf{q}_{23}} S(\mathbf{q}_{23}; \mathbf{r}_{23}, \mathbf{r}_{13}) = 0. \quad (\text{A9})$$

The saddle points are given by

$$\mathbf{q}_{23} = \mathbf{q}_{23}^{(o)} \equiv i2\mu_{(31)2}\sqrt{\varepsilon_a} \frac{\mathbf{r}_{23} - \lambda_1\mathbf{r}_{13}}{R(\mathbf{r}_{23}, \mathbf{r}_{13})}, \quad (\text{A10})$$

where

$$R(\mathbf{r}_{23}, \mathbf{r}_{13}) = \sqrt{2\mu_{31}r_{13}^2 + 2\mu_{(31)2}(\mathbf{r}_{23} - \lambda_1\mathbf{r}_{13})^2} \quad (\text{A11})$$

$$\equiv \sqrt{2\mu_{23}r_{23}^2 + 2\mu_{(23)1}(\mathbf{r}_{13} - \lambda_2\mathbf{r}_{23})^2} \quad (\text{A12})$$

is the hyperradius R . Whereas

$$\mathbf{q}_{13} = \mathbf{q}_{13}^{(o)} \equiv \hat{\mathbf{r}}_{13}q'_{13}^{(o)}(q_{23}) - \lambda_1\mathbf{q}_{23}^{(o)} \quad (\text{A13})$$

at $\varepsilon = \varepsilon_a$, from the relations (A10) and (A13), one obtains

$$\mathbf{q}_{13}^{(o)} = i2\mu_{(23)1}\sqrt{\varepsilon_a} \frac{\mathbf{r}_{13} - \lambda_2\mathbf{r}_{23}}{R(\mathbf{r}_{23}, \mathbf{r}_{13})}. \quad (\text{A14})$$

An asymptotic expression sought by us is generated by contributions from the saddle points $\mathbf{q}_{23} = \mathbf{q}_{23}^{(o)}$. To this end, we can employ the following standard techniques in the r.h.s. of (A6). Firstly, the part C of the integration region containing the vicinity of the saddle points $\mathbf{q}_{23} = \mathbf{q}_{23}^{(o)}$ is separated, i.e. $\{q_{23;1}^{(o)}, q_{23;2}^{(o)}, q_{23;3}^{(o)}\} \in C$, where $q_{23;j}^{(o)}$ ($j=1,2$ and 3) is a corresponding coordinate of the vector $\mathbf{q}_{23}^{(o)}$. Then, the leading term of the r.h.s. of (A6) at $r_{13} \rightarrow \infty$ can be found by using the following formula (1.10') of Section 3 of the Chapter 4 of Ref.[34]:

$$\int d\mathbf{q}_{23} e^{r_{13}S(\mathbf{q}_{23};\mathbf{r}_{23},\mathbf{r}_{13})} h(\mathbf{q}_{23};\mathbf{r}_{23},\mathbf{r}_{13}) \simeq \int_C d\mathbf{q}_{23} e^{r_{13}S(\mathbf{q}_{23};\mathbf{r}_{23},\mathbf{r}_{13})} h(\mathbf{q}_{23};\mathbf{r}_{23},\mathbf{r}_{13}) \quad (\text{A15})$$

$$\simeq \left(\frac{2\pi}{r_{13}}\right)^{3/2} e^{r_{13}S(\mathbf{q}_{23}^{(o)};\mathbf{r}_{23},\mathbf{r}_{13})} \left[\det \left\| -\frac{\partial^2}{\partial q_{23;i} \partial q_{23;j}} S(\mathbf{q}_{23};\mathbf{r}_{23},\mathbf{r}_{13}) \right\|_{\mathbf{q}_{23}=\mathbf{q}_{23}^{(o)}} \right]^{-1/2} \times h(\mathbf{q}_{23}^{(o)};\mathbf{r}_{23},\mathbf{r}_{13}) \quad (\text{A16})$$

for $r_{13} \rightarrow \infty$, where $q_{23;j}$ ($j=1, 2$, and 3) is a corresponding coordinate of the vector \mathbf{q}_{23} .

As a result, from Eqs.(A6)–(A8), (A15) and (A16) the proper three-body asymptotics of the total wave function $\Psi(\mathbf{r}_{23},\mathbf{r}_{13})$ $r_{13} \rightarrow \infty$ can be obtained as

$$\Psi_a(\mathbf{r}_{23},\mathbf{r}_{13}) \simeq \Psi_a^{(as)}(\mathbf{r}_{23},\mathbf{r}_{13}) = C_a(r,\hat{\mathbf{r}}_{23},\hat{\mathbf{r}}_{13})(2\sqrt{\varepsilon_a}R)^{-\eta_a(r,\hat{\mathbf{r}}_{23},\hat{\mathbf{r}}_{13})} \times e^{-\sqrt{\varepsilon_a}R}/R^{5/2}. \quad (\text{A17})$$

Herein

$$C_a(r,\hat{\mathbf{r}}_{23},\hat{\mathbf{r}}_{13}) = -\frac{(m\sqrt{\varepsilon_a})^{3/2}}{\sqrt{2}\pi^{5/2}} W(-\mathbf{q}_{23}^{(o)}, -\mathbf{q}_{13}^{(o)}) \quad (\text{A18})$$

is the three-body asymptotic normalization factor, $R \equiv R(\mathbf{r}_{23},\mathbf{r}_{13})$ and

$$\eta_a(r,\hat{\mathbf{r}}_{23},\hat{\mathbf{r}}_{13}) = iz_3z_1e^2\mu_{13}/q_{13}^{(o)}. \quad (\text{A19})$$

Recall that the function $W(-\mathbf{q}_{23}^{(o)}, -\mathbf{q}_{13}^{(o)})$ is the total OSVF for the virtual decay (11) because when $\mathbf{q}_{23} = \mathbf{q}_{23}^{(o)}$ and $\mathbf{q}_{13} = \mathbf{q}_{13}^{(o)}$, the particles 1, 2 and 3 are on the mass shell.

It should be noted that the asymptotic formula is also valid for $r_{23} \rightarrow \infty$. This point can be easily shown if permutation of the order of integration over \mathbf{q}_{13} and \mathbf{q}_{23} is done in (A1). As a result, one obtains the same asymptotic formula (A17). This means that asymptotic formula (A17) is valid when both r_{23} and r_{13} (or R) tend to infinity.

The expression (A17) coincides with the asymptotic expression obtained in Ref.[30] for $\Psi(\mathbf{R})$ at $R \rightarrow \infty$ if in the latter a value of the charge ($z_b \equiv z_2$) for the particle 2 is put to zero, the three-body asymptotic normalization factor $C(\hat{\mathbf{R}})$ is substituted by $C(r,\hat{\mathbf{r}}_{23},\hat{\mathbf{r}}_{13})$ and the hyperradius R is determined by either Eq.(A11) or Eq.(A12). It follows from here that the limit $R \rightarrow \infty$ for the asymptotic expression obtained in Ref.[30] indeed means that both r_{23} and r_{13} tend simultaneously to infinity.

APPENDIX B: APPROXIMATE THREE-BODY WAVE FUNCTIONS

Below, we briefly present the idea and the essential formulas of the aforementioned Lagrange-mesh technique utilized by D. Baye [27] for the halo ($E^*=3.562$ MeV) state of ${}^6\text{Li}$.

According to Ref.[41], the Hamiltonian describing the relative motion of the nucleons with respect to the core (α -particle) reads

$$H = \frac{\hat{\mathbf{q}}_{p\alpha}^2}{2\mu_{p\alpha}} + \frac{\hat{\mathbf{q}}_{n\alpha}^2}{2\mu_{n\alpha}} + \frac{\hat{\mathbf{q}}_{p\alpha}\hat{\mathbf{q}}_{n\alpha}}{5\mu_{p\alpha}} + V_{p\alpha} + V_{n\alpha}^N + V_{np}^N, \quad (B1)$$

where $V_{ij} = V_{ij}^N + V_{ij}^C$ and $V_{ij}^N(V_{ij}^C)$ is the nuclear(Coulomb) potential between the centers of mass of particles i and j . The eigenvalue of H provides a binding energy of the ${}^6\text{Li}(E^*=3.562)$ state in the $(p+n+\alpha)$ -channel. According to [27], the central part of the Minnesota NN potential with an exchange parameter $u=1$ [42] and two kinds of the αN potential were employed. The latters are taken from Ref.[21] (the M1 model), which takes into account the exchange Majorana component both in the central and the spin-orbit term, and from Ref.[23] (the M2 model) with the the central and the spin-orbit terms. In (B1), they are both expressed as sums of Gaussians, in which, similar to Ref.[43], the pseudopotential technique is also applied in [27] to eliminate the forbidden s state of the αN interaction, which stimulates the Pauli antisymmetrization principle between the nucleon and the core.

Within the framework of the Lagrange-mesh technique [36–39], a partial wave of the $pn\alpha$ wave function for the second excited state of the ${}^6\text{Li}$ nucleus is presented as

$$\Psi_{LS}(r_{23}, r_{13}) = (r_{23}r_{13})^{-1} \sum_{i_1, i_2=1}^N c_{i_1 i_2}^{LS} F_{i_1 i_2}(r_{23}, r_{13}). \quad (B2)$$

In this expression, the $F_{i_1 i_2}$ are Lagrange basis functions and the $c_{i_1 i_2}^{LS}$ are variational coefficients. Since the total angular momentum J of the halo ($E^*=3.562$ MeV) state of ${}^6\text{Li}$ is zero, its total orbital moment L and its total spin S are equal ($L=S=0$ or 1). As the parity is positive, the relative orbital moments l_{23} and l_{13} take the common value l . The two-dimensional Lagrange functions have the following form

$$F_{i_1 i_2}(r_{23}, r_{13}) = f_{i_1}(r_{13}/h) f_{i_2}(r_{23}/h)/h. \quad (B3)$$

Here

$$f_i(x) = (-1)^i x_i^{-1/2} x(x-x_i)^{-1} L_N(x) e^{-x/2} \quad (B4)$$

is the one-dimensional Lagrange-Laguerre function, where $L_N(x)$ is a Laguerre polynomial and the Laguerre zeros x_i are solution of $L_N(x_i)=0$ [22, 36]. The basis functions $F_{i_1 i_2}(r_{23}, r_{13})$ are associated with N^2 mesh points (hx_{i_1}, hx_{i_2}) where they satisfy the Lagrange property

$$F_{i_1 i_2}(hx_{i'_1}, hx_{i'_2}) \propto \delta_{i_1 i'_1} \delta_{i_2 i'_2}.$$

The normalization conditions for the radial wave functions and for the coefficients $c_{i_1 i_2}^{LS}$ at Gauss approximation are given by Eqs.(36) and (37) of Ref.[18], respectively. The scale factor h is a non-linear variational parameter aimed at adjusting the mesh to the domain of physical interest.

The values of the coefficients $c_{i_1 i_2}^{LS}$ were obtained by D. Baye [27] for the both aforesaid kinds of the αN potential (the M1 and M2 models). Nevertheless one should note only the following main points. To approximately reproduce the experimental binding energy 0.136 MeV of the second excited state

of ${}^6\text{Li}$, the potentials of Refs.[21] and [23] were multiplied by 1.08 and by 1.01, respectively, as it was also done in Ref.[18]. Then, the binding energy was calculated as 0.1365 MeV for the αN potential Ref.[21] in the M1 model and as 0.1323 MeV for that from Ref.[23] in the M2 model. The Coulomb αp interaction was represented by $2e^2\text{erf}(0.83r)/r$ and took into account the finite extension of the α particle. The corresponding wave functions contained partial waves $l=0$ to 18 and were obtained with $h = 0.3$ and 0.4 fm for the αN potential of the M1 model and the M2 model, respectively. The calculations were performed with $N=28$, i.e. 784 basis states per partial wave for a total of 29008 basis states, for each of the αN potentials. The dominant partial waves for the considered ${}^6\text{Li}$ nucleus were, in decreasing order of importance, $(L,l)=(0,1)$, $(1,1)$, $(0,2)$, $(0,0)$ and $(1,2)$. The respective probabilities were 84.6%, 8.4%, 3.8% and 2.2% for the M1 model and 79.1%, 15.8%, 3.1% and 1.6% for the M2 model [27].

References

- [1] M. V. Zhukov, B. V. Danilin, D. V. Fedorov, J. M. Bang, I. J. Thompson, J. S. Vaagen, Phys. Rep. 231 (1993) 151.
- [2] A. C. Mueller, B. M. Sherrill, Ann. Rev. Nucl. Part. Sci. 43 (1993) 529.
- [3] D. Baye, M. Kruglansky, M. Vincke, Nucl. Phys. A 573 (1994) 431.
- [4] P. G. Hansen, Nucl. Phys. A 588 (1995) 1.
- [5] I. Tanihata, J. Phys. G. 22 (1996) 157.
- [6] B. Jonson, Nucl. Phys. A 547 (1994) 151.
- [7] P. Descouvemont, Nucl. Phys. A 626 (1997) 647.
- [8] T. Myo, K. Kato, S. Aoyama, K. Iketa, Phys. Rev. C 63 (2001) 054313.
- [9] I. J. Thompson, Nucl. Phys. A 701 (2002) 7.
- [10] H. Esbensen, K. Hagino, P. Mueller, H. Sagawa, Phys. Rev. C 76 (2007) 024302.
- [11] K. Hagino, H. Sagawa, T. Nakamura, S. Shimoura, Phys. Rev. C 80 (2009) 031301.
- [12] B. E. Grinyuk, I. V. Simenog, Yad. Fiz. 72 (2009) 10.
- [13] I. Tanihata, H. Savajols, R. Kanungo, Prog. Part. Nucl. Phys. 68 (2013) 215.
- [14] S. P. Merkur'ev, Yad. Fiz. 19 (1974) 447[Sov.J. Nucl. Phys. 19 (1974) 222].
- [15] L. D. Blokhintsev, M. K. Ubaidullaeva, R. Yarmukhamedov, Phys. At. Nucl. 62 (1999) 1289.
- [16] R. Yarmukhamedov, M. K. Ubaidullaeva, Int. J. Mod. Phys. E 18 (2009) 1561.
- [17] L. D. Blokhintsev, M.K. Ubaidullaeva, R. Yarmukhamedov, Phys. At. Nucl. 68 (2005) 1372.
- [18] R. Yarmukhamedov, D. Baye , Ch. Leclercq-Willain, Nucl. Phys. A 705 (2002) 335.
- [19] R. Yarmukhamedov, J. Phys.:Conference Series. 569 (2014) 012037.
- [20] V. I. Kukulín, V. N. Pomerantsev, Kh. D. Razikov, V. T. Voronchev, G. G. Ryzhikh, Nucl. Phys. A 586 (1995) 151.
- [21] V. T. Voronchev, V. I. Kukulín, V. N. Pomerantsev, G. G. Ryzhikh, Few-Body System. 18 (1995) 191.
- [22] D. Baye, Nucl. Phys. A 627 (1997) 305.
- [23] H. Kanada, T. Kaneko, S. Nagata, M. Nomoto, Prog. Theor. Phys. 61 (1979) 1327.
- [24] L. D. Blokhintsev, I. Borbely, E. I. Dolinskii, Sov. J. Part. Nucl. 8 (1977) 485.
- [25] M. P. Locher, T. Mizutani, Phys. Rep. 46 (1978) 43.

- [26] L. D. Blokhintsev, A. M. Mukhamedzhanov, R. Yarmukhamedov, Eur. Phys. J. A 49 (2013) 108.
- [27] D. Baye, privated communication(unpublished).
- [28] L. D. Blokhintsev, E. I. Dolinskii, Yad. Fiz. 5 (1967) 797[Sov.J. Nucl. Phys. 5 (1967) 565].
- [29] E. I. Dolinskii, A. M. Mukhamedzhanov, Yad. Fiz. 3 (1966) 252[Sov.J. Nucl. Phys. 3 (1966) 180]
- [30] A. M. Mukhamedzhanov, M. K. Ubaidullaeva, R. Yarmukhamedov, Teor. i Mat. Fiz. 94 (1993) 448[Theor. and Math. Phys. 94 (1993) 315].
- [31] M. Abramowitz , I.A. Stegun, Handbook of Mathematical Function, Dover, NewYork, 1970.
- [32] A. Kratzer, W. Franz, Transzendente funktionen. Hamburg, Leipzig 1960, Akademische Verlags-
gesellschaft.
- [33] H. Bateman, A. Erdelyi. Higher transcendental functions, vol.1, New York Toronto London MC
Graw-Hill Book Company, ING, 1953.
- [34] M. Fedoryuk. Metod perevala (Saddle method), Moscow, Nauka, 1977 (Russia).
- [35] G. V. Avakov, S. N. Belolipetskii, L. D. Blokhintsev, G. V. Valiev, I. R. Gulamov, Yu. I. Denisov,
T. Iskhakov, A. M. Mukhamedzhanov, E. A. Romanovskii, R. Yarmukhamedov, Yad.Fiz.47 (1988)
1508[Sov.J.Nucl.Phys. 47 (1988) 957].
- [36] M. Vincke, L. Malegat, D. Baye, J. Phys. B 26 (1993) 811.
- [37] D. Baye, P.-H. Heenen, J. Phys. A 19 (1986) 2041.
- [38] D. Baye, M. Vincke, Phys. Rev. E 59 (1999) 7195.
- [39] D. Baye, Phys. Rep. 565 (2015) 1.
- [40] S.P. Merkur'ev and L.D. Faddeev, Kvantovaya teoriya rasseyaniya dlya sistem neskol'kih chastits,
M:Nauka, Redaktsiya fiz.-mat. literatura, Moskva, 1985.
- [41] Y. Suzuki, Nucl.Phys. A 528 (1991) 395; private communication.
- [42] Y. T. Tang, M. LeMere, D.R. Thompson, Phys.Rep. 47 (1978) 167.
- [43] V. M. Krasnopol'skii, V.I. Kukulin, Sov. J. Nucl. Phys., 20 (1975) 470.

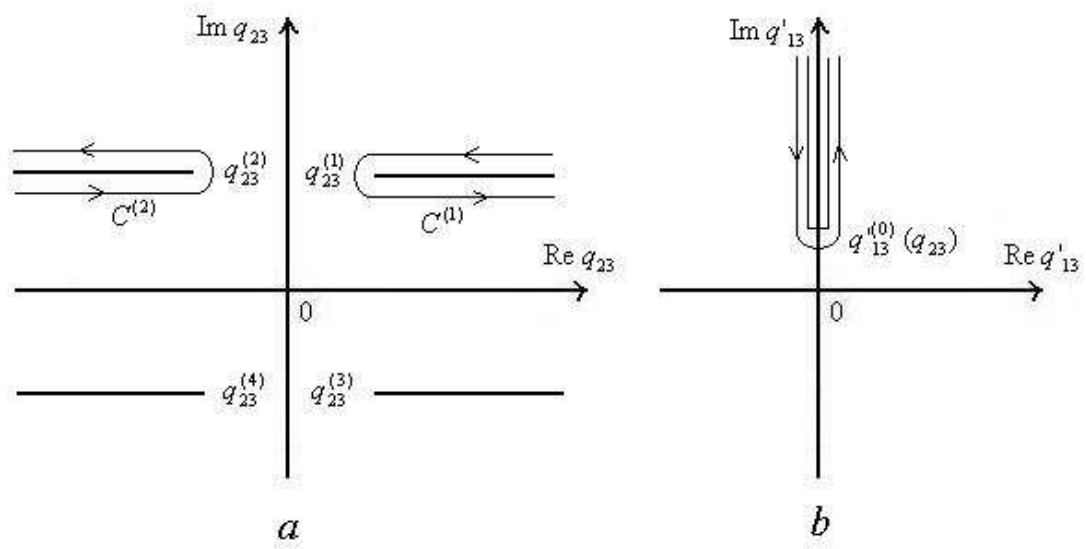


Figure 1: Contours in the q_{23} and q'_{13} complex planes.

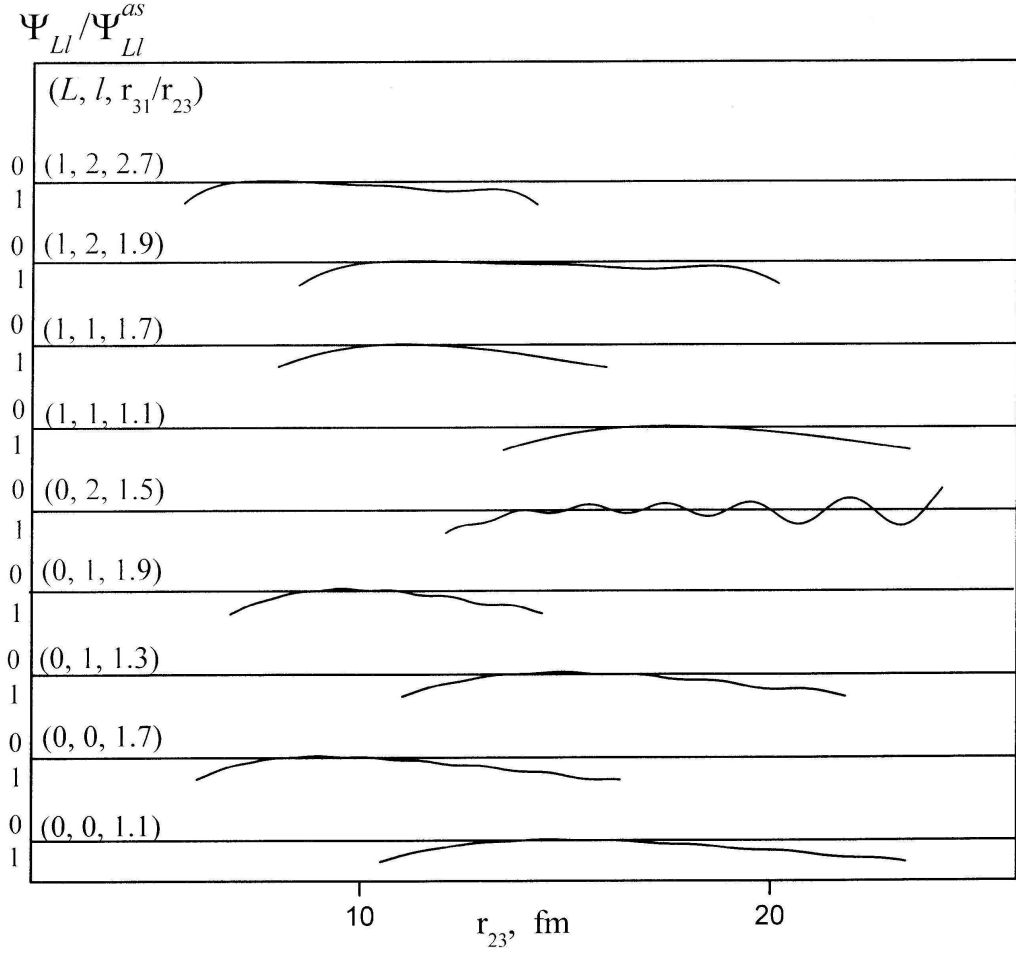


Figure 2: Ratio of the numerical partial wave functions (??) to the asymptotic expression (29) as a function of r_{23} for fixed values of the coordinate ratio $r = r_{13}/r_{23}$. Each case is calculated for the (r_{23}, r_{13}) pair of fitting points which provides the corresponding values $C_{Ll}^{(j)}(r)$ obtained by means of the fitting procedure mentioned above.

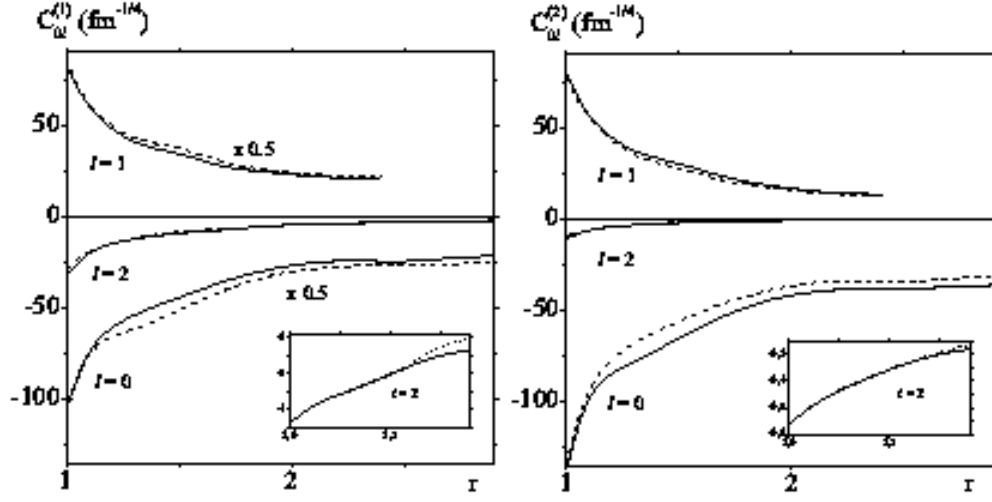


Figure 3: The recommended values of the function $C_{Ll}^{(j)}(r)$ for $L=0$ and $l=0, 1$ and 2 ($j=1$ and 2). The solid and dashed lines correspond to the M1 and M2 models, respectively. The uncertainty for each the curve is within up to $\pm 10\%$.

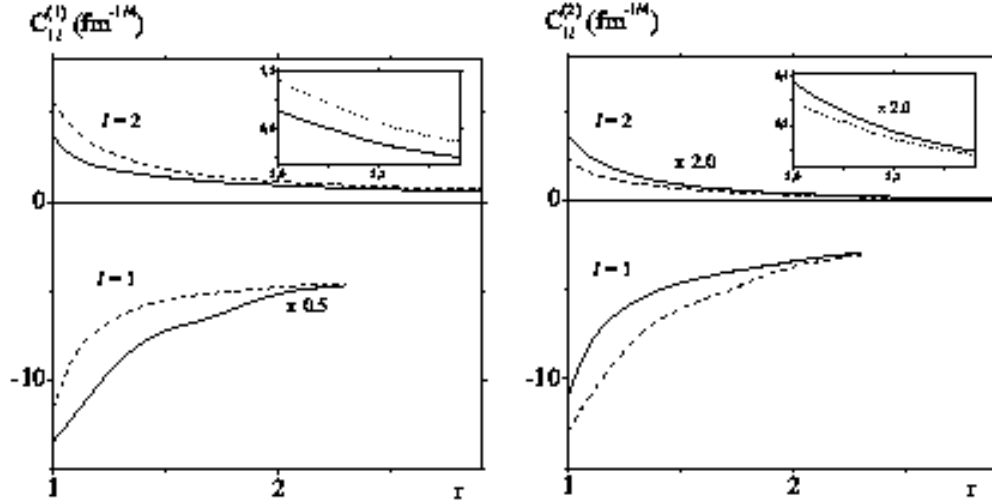


Figure 4: Same as Fig.2 for $L=S=1$ and $l=1$ and 2 .

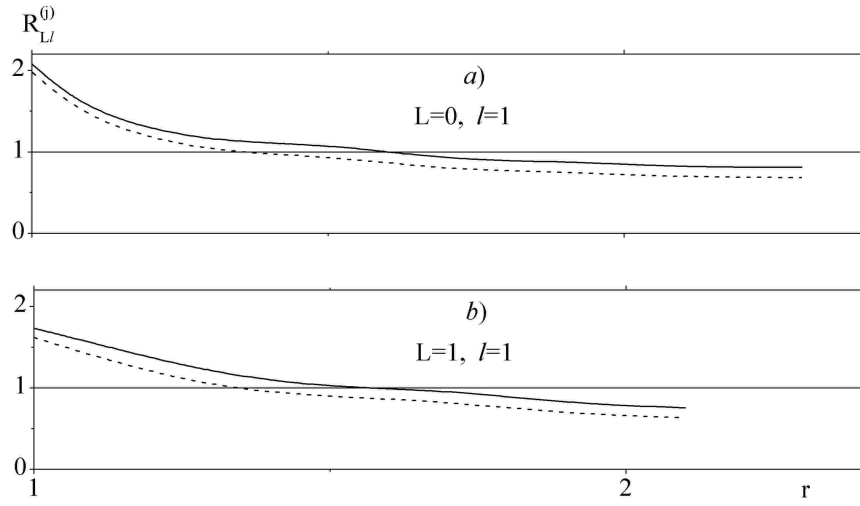


Figure 5: The ratio $R_{Ll}^{(j)}$ of the TBANFs derived for the ${}^6\text{Li}(3.562 \text{ MeV}, J^\pi=0^+, T=1)$ nucleus to those for ${}^6\text{He}(\text{g.s.}, J^\pi=0^+, T=1)$ nucleus as a function of r for the M2 model. The solid and dashed lines correspond to $j=1$ and 2 , respectively. The data for ${}^6\text{He}(\text{g.s.}, J^\pi=0^+, T=1)$ are taken from [18].

Table 1: The three-body asymptotic normalization functions $C_{Ll}^{(1)}$, $C_{Ll}^{(2)}$ for the halo ($E^*=3.562$ MeV; $J^\pi=0^+$; $T=1$) state of ${}^6\text{Li}$, ratios $C_{Ll}^{(2)}/C_{Ll}^{(1)}$ and the width of an interval for the variable r_{23} (Δ) within which the expressions (29) and (B2) agree within 10% for different choices of the matching points (r_{23}, r_{13}) and $(r_{23} + \Delta r_{23}, r_{13} + \Delta r_{13})$ at fixed values of the ratio $r = r_{13}/r_{23}$ for the quantum numbers $L=0, 1$ and $l=0, 1$ and 2 .

(L, l)	r	r_{23} fm	r_{13} fm	Δr_{23} fm	M1 model				M2 model			
					Δ fm	$C_{Ll}^{(1)}$ fm $^{-1/4}$	$C_{Ll}^{(2)}$ fm $^{-1/4}$	$C_{Ll}^{(2)}/C_{Ll}^{(1)}$	Δ fm	$C_{Ll}^{(1)}$ fm $^{-1/4}$	$C_{Ll}^{(2)}$ fm $^{-1/4}$	$C_{Ll}^{(2)}/C_{Ll}^{(1)}$
1	2	3	4	5	6	7	8	9	10	11	12	13
(0,0)	1.1	14.00	15.40	2.000	10.0	-130	-86.7	0.666	13.0	-132	-84.6	0.643
		14.25	15.68		10.2	-125	-83.7	0.672	13.1	-127	-82	0.647
		13.75	15.13	2.250	10.0	-133	-87.9	0.664	12.8	-135	-86.6	0.639
		14.25	15.68		10.2	-122	-82.5	0.675	13.3	-124	-80.5	0.659
	1.3	10.25	13.33	2.000	8.9	-127	-79.8	0.630	10.6	-107	-67.4	0.628
		10.75	13.98		9.1	-116	-74.4	0.639	11.2	-100	-63.7	0.635
		10.25	13.33	2.250	8.9	-125	-78.9	0.631	11.0	-105	-66.0	0.630
		10.75	13.98		9.2	-113	-72.8	0.642	11.2	-100	-63.7	0.635
	2.5	5.50	13.75	2.000	5.2	-59.4	-41.9	0.706	6.4	-53.1	-37.0	0.698
		6.00	15.00		5.4	-53.9	-38.5	0.716	6.4	-50.3	-35.4	0.703
		5.50	13.75	2.250	5.3	-58.8	-41.5	0.706	6.5	-51.6	-36.1	0.700
		6.00	15.00		5.5	-52.0	-37.4	0.719	6.5	-50.0	-35.1	0.703
(0,1)	1.1	16.00	17.60	2.000	6.7	127	58.0	0.455	8.0	136	61.1	0.449
		16.50	18.15		6.6	117	53.7	0.459	8.2	124	56.2	0.452
		16.00	17.60	2.250	8.3	125	57.1	0.456	9.6	134	60.3	0.449
		16.50	18.15		8.4	117	53.5	0.459	10.6	119	54.1	0.453
	1.5	10.25	15.38	2.000	6.2	82.4	33.0	0.401	6.6	79.8	31.8	0.398
		10.75	16.13		6.3	77.0	31.0	0.403	7.8	70.7	28.4	0.401
		10.25	15.38	2.125	6.3	81.5	32.7	0.401	6.7	78.9	31.4	0.398
		10.75	16.13		6.4	76.6	30.9	0.403	8.0	69.5	27.9	0.402

Table 2: Table 1(continue)

(L, l)	r	r_{23} fm	r_{13} fm	Δr_{23} fm	$M1$ -model				$M2$ -model			
					Δ fm	$C_{Ll}^{(1)}$ fm $^{-1/4}$	$C_{Ll}^{(2)}$ fm $^{-1/4}$	$C_{Ll}^{(2)}/C_{Ll}^{(1)}$	Δ fm	$C_{Ll}^{(1)}$ fm $^{-1/4}$	$C_{Ll}^{(2)}$ fm $^{-1/4}$	$C_{Ll}^{(2)}/C_{Ll}^{(1)}$
1	2	3	4	5	6	7	8	9	10	11	12	13
(0,1)	2.4	6.25	15.00	2.000	5.1	49.3	14.4	0.292	5.6	48.7	14.2	0.290
		6.75	16.20		5.1	44.4	13.0	0.294	5.6	43.3	12.6	0.292
		6.25	15.00	2.125	5.2	48.4	14.1	0.292	5.6	48.4	14.1	0.291
		6.75	16.20		5.1	44.1	13.0	0.294	6.4	42.2	12.4	0.292
(0,2)	1.3	17.00	22.10	2.000	7.0	-11.2	-3.07	0.274	12.3	-12.7	-3.43	0.270
		17.50	22.75		6.8	-11.6	-3.18	0.274	12.5	-11.6	-3.16	0.272
		17.00	22.10	2.250	7.1	-11.7	-3.21	0.273	12.4	-11.1	-3.03	0.272
		17.50	22.75		6.8	-11.9	-3.25	0.273	12.4	-11.5	-3.12	0.272
	1.9	10.00	19.00	2.000	6.6	-5.06	-0.895	0.177	12.0	-4.97	-0.877	0.177
		10.50	19.95		6.5	-4.89	-0.867	0.177	11.7	-4.76	-0.841	0.177
		10.00	19.00	2.250	6.6	-4.91	-0.870	0.177	11.9	-5.05	-0.891	0.176
		10.50	19.95		6.5	-5.11	-0.905	0.177	11.5	-4.41	-0.780	0.177
(1,1)	1.0	18.00	18.00	2.000	7.5	-23.8	-11.3	0.477	10.5	-27.6	-13.3	0.481
		18.50	18.50		7.5	-22.2	-10.6	0.480	11.1	-25.6	-12.4	0.484
		18.00	18.00	2.250	7.5	-23.4	-11.2	0.478	10.7	-27.1	-13.1	0.482
		18.50	18.50		7.6	-21.5	-10.3	0.481	11.4	-25.1	-12.2	0.485
	1.7	10.00	17.00	2.000	6.7	-11.2	-4.40	0.393	8.0	-14.3	-5.59	0.390
		10.50	17.85		6.9	-10.1	-4.00	0.398	8.5	-13.0	-5.12	0.394
		10.00	17.00	2.125	6.7	-11.1	-4.35	0.393	8.1	-14.2	-5.53	0.390
		10.50	17.85		6.9	-9.87	-3.94	0.399	8.6	-12.9	-5.07	0.395
	1.3	16.50	21.45	2.000	7.1	1.72	0.467	0.272	12.1	2.52	0.680	0.270
		17.50	22.75		6.9	1.70	0.461	0.272	12.6	2.35	0.636	0.271
		16.50	21.45	2.250	7.1	1.71	0.466	0.272	12.1	2.49	0.674	0.270
		17.50	22.75		7.0	1.72	0.467	0.272	12.6	2.34	0.633	0.271
	1.9	10.00	19.00	2.000	6.8	1.02	0.180	0.177	11.5	1.26	0.223	0.177
		12.00	22.80		6.6	1.01	0.178	0.177	11.4	1.20	0.212	0.177
		10.00	19.00	2.250	6.7	1.000	0.178	0.177	11.5	1.25	0.221	0.177
		12.00	22.80		6.5	0.987	0.175	0.177	11.5	1.20	0.212	0.177